

# UC Merced

## UC Merced Previously Published Works

### Title

Effect of Aliphatic Chain Length on the Stress-Strain Response of Semiaromatic Polyamide Crystals

### Permalink

<https://escholarship.org/uc/item/0f57g5fb>

### Journal

Macromolecules, 55(12)

### ISSN

0024-9297

### Authors

Yang, Quanpeng  
Li, Wenjun  
Stober, Spencer T  
[et al.](#)

### Publication Date

2022-06-28

### DOI







10.1021/acs.macromol.2c00081

### Supplemental Material

<https://escholarship.org/uc/item/0f57g5fb#supplemental>

Peer reviewed

# Effect of Aliphatic Chain Length on the Stress-strain Response of Semi-aromatic Polyamide Crystals

Quanpeng Yang <sup>†</sup>, Wenjun Li <sup>‡</sup>, Spencer T. Stober <sup>‡</sup>, Adam B. Burns <sup>‡</sup>, Manesh  
Gopinadhan <sup>‡</sup> and Ashlie Martini <sup>\*,†</sup>

<sup>†</sup>*Department of Mechanical Engineering, University of California-Merced, 5200 N.  
Lake Road, Merced, California 95343, United States*

<sup>‡</sup>*Corporate Strategic Research, ExxonMobil Research and Engineering Company, 1545  
Route 22 East, Annandale, New Jersey 08801, United States*

E-mail: [amartini@ucmerced.edu](mailto:amartini@ucmerced.edu)

## Abstract

Reactive molecular dynamics simulations were used to model poly(*p*-phenylene terephthalamide) and related aromatic-aliphatic polyamides derived from *p*-phenylene diamine and aliphatic diacids with different numbers of carbon atoms in the aliphatic chain (5, 6, 7, or 8). Tensile strain was applied to each polymer crystal in the chain direction and the mechanical response was characterized. All the polymers with aliphatic segments exhibited strain hardening, transitioning from an initial (low-strain) linear regime to a second (high-strain) linear regime. The modulus at high strain was similar for all polymers, but the modulus calculated at low strain decreased with increasing aliphatic chain length. The decrease in the low-strain modulus with increasing chain length was explained by the observation that polymers with longer aliphatic chains were wavier (i.e., deviated more from the fully extended conformation) in the quiescent

state such that they could accommodate low strain without deforming covalent bonds. Extension of wavy chains occurred through an intra-chain process for all polymers, quantified by the bond dihedral angles. In addition, for polymers with an even number of non-aromatic carbons, the strain response involved slip between chains within the hydrogen bonded sheets. The ultimate stress of the polymers exhibited an odd-even effect (even polymers were weaker) which was explained by differences in hydrogen bonding and ring-ring coplanarity prior to failure; polymers with an even number of carbon atoms had less favorable H-bonding and poorer ring alignment. The results revealed direct correlations between aliphatic chain length, intra- and inter-chain interactions, and the mechanical properties of polyamide crystals.

## Introduction

Aromatic polyamides (i.e., aramids), the most famous of which is poly(*p*-phenylene terephthalamide) (PPTA), are well-known for their excellent mechanical properties (superior strength-to-weight ratio and flexibility),<sup>1,2</sup> thermal stability (thermal decomposition temperature of 500° C),<sup>3,4</sup> and chemical resistance (to acid, alkali and organic solvents).<sup>5-9</sup> These properties make PPTA ideal for many different uses, including aerospace and military applications (e.g., bulletproof body armor fabric and ballistic composites) where performance-to-weight ratio is critical.<sup>10-13</sup>

However, there are limitations of PPTA, primarily associated with processability due to its high melting temperature ( $\sim 500$  °C) and poor solubility (only soluble in aggressive polar solvents, such as concentrated sulfuric acid). These make the processing of PPTA challenging, expensive, and environmentally unfriendly, and directly limit its broader application.<sup>14-19</sup>

Extensive research has been conducted to develop materials with properties comparable to PPTA but with potentially better processability.<sup>20</sup> The high melting temperature of PPTA is a result of its rigid and extended conformation, which is due to the rigidity of the aramid

backbone and strong intermolecular interactions—hydrogen bonding (H-bonding) and  $\pi$ -stacking.<sup>11,21–24</sup> A variety of methods have been attempted using chemical modification to lower the melting temperature, including introducing bulky, packing-disruptive groups into the polymer chain or as side-groups, incorporating flexible groups into the polymer backbone, and using *meta*-substituted or otherwise asymmetric monomers.<sup>25–32</sup> One such approach is to combine the rigidity of aromatic moieties and the flexibility of aliphatic moieties to create so-called aromatic-aliphatic polyamides.<sup>11,20,33–38</sup>

It is expected that even minor changes in the molecular structure of the aromatic-aliphatic polyamides might significantly affect the mechanical behavior. For example, longer spacer lengths for a given aromatic amide system leads to a reduction in hydrogen bond density which will lower the melting temperature.<sup>20</sup> However, experimentally studying this relationship for polyamide crystals is difficult and time-consuming, and requires sensitive equipment.<sup>5,39,40</sup> Obtaining large single crystal materials is challenging (slow evaporation of solvent is used to get large single crystals for modulus measurements<sup>41–43</sup>), and the morphology of the polymers is complicated due to the presence of amorphous contributions (e.g., non-crystalline regions and defects). In addition, it is difficult with experimental techniques to distinguish the relative contributions of intramolecular (e.g., covalent bonds) interactions and intermolecular interactions (e.g., H-bonding and  $\pi$ -stacking) to bulk mechanical properties.<sup>44</sup>

To overcome these limitations, experimental methods have been complemented by molecular dynamics (MD) simulations to study materials at the atomistic scale.<sup>5</sup> MD simulations can help interpret experimental results, guide the development of new experimental methods, and provide useful information about both the dynamic and static properties of molecular systems.<sup>45–47</sup> MD simulations have been successfully applied to study aromatic-aliphatic polyamide crystals, including the role of aliphatic and aromatic groups on intermolecular interactions, free volume, and glass transition temperature,<sup>32,48</sup> the origin of melting,<sup>11</sup> and the influence of methylene segments on crystal packing and chain conformation.<sup>11</sup> Understanding

the relationship between chemical structure and the emergent physical properties will enable chemists to synthesize polymers with desired thermo-mechanical properties. However, MD simulations have not been used to understand the effect of the length of flexible aliphatic moieties on the mechanical properties of semi-aromatic polyamide crystals. In our previous study,<sup>49</sup> we compared PPTA with one PPTA-related aromatic-aliphatic polyamide, PAP5, where 5 refers to the number of carbon atoms in the diacid monomer used in the reaction with *p*-phenylene diamine. The results showed that some mechanical properties (tensile strength and failure strain) of PAP5 were superior to those of PPTA.

Here, we extended our previous study by modeling PPTA and a homologous set of PPTA-related aromatic-aliphatic polyamides—PAP5, PAP6, PAP7, and PAP8—with 5, 6, 7 or 8 carbon atoms in the diacid monomer. The goal was to characterize the effect of aliphatic chain length on mechanical properties and then correlate differences between polymers to intra- and inter-molecular interactions. Reactive MD simulations showed that the polymer crystals had lower stiffness in the chain direction at low strain than high strain, and the length of the aliphatic segment affected both the low-strain elastic modulus and ultimate stress. The difference between low- and high-strain behavior was attributed to the configurations of the chains in the quiescent state and the aliphatic chain length effect was found to be caused by both intra- and intra-chain processes.

## Methods

The polymer crystal models were initially constructed using Materials Studio.<sup>50</sup> Unit cell dimensions were initialized based on the models for PPTA and PAP5 derived by Ref. 11 using a combination of X-ray scattering and molecular modeling (albeit with a different force field than the one used herein). The crystal structures of PAP6 (which is reported in Ref. 11) and PAP7 and PAP8 (for which there is no experimental data) were initialized based on the lattice parameters of PAP5 by simply extending the aliphatic chain length

and the unit cell in the chain direction (*c*-axis) correspondingly. This approach reproduces the salient intra- and intermolecular features of the structures elucidated in Ref. 11. All five polyamide crystals exhibit two-dimensional, alternately sheared H-bonded sheets ( $\alpha$  form) with the carbonyls on each diacid oriented in the same direction for the odd polymers (PAP5 and PAP7) and in opposite directions for the even polymers (PAP6 and PAP8). Moreover, the *c*-axis dimensions of PPTA, PAP5, and PAP6 agree quantitatively (within 1 Å) and comprise the same number of repeats, indicating that the chain conformation, particularly those of the aliphatic segments, are consistent with the literature. There are some differences in the positions of the aromatic rings. Ref. 11 reports an alternating twist of the phenyl rings and a translation along the *c*-axis (pseudomonoclinic), which our model does not include. Nevertheless, both models exhibit  $\pi$ - $\pi$  registry between neighboring chains. Having no experimental basis for initializing the crystal structures of PAP7 and PAP8, we elect to preserve the aforementioned features by using the same scheme for all four semiaromatic polyamides.

The lattice parameters of the initial unit cells are given in Table S1. The chemical formulas and atomic-scale models of the PPTA and PAP5-PAP8 unit cells are shown in Figure 1. The chain direction was aligned with the *x*-axis (corresponding to crystallographic axis *c*), and the H-bonding and  $\pi$ -stacking directions were aligned with the *y*- and *z*-axes, respectively. The unit cell was then replicated in the *x*-, *y*- and *z*-directions to create larger simulation boxes (4×4×4) to maintain MD simulation fidelity while maximizing the computational efficiency, as demonstrated in our previous work.<sup>49</sup> Periodic boundary conditions were applied in all three directions to mimic ideal crystalline polymers with infinite chain length and without defects or chain ends. Although the models in this study are approximations of realistic crystalline polymers that have finite length chains with defects and chain ends, the results here represent upper bounds on the mechanical properties and the simulation methods developed form the basis for more realistic models.

In our previous study,<sup>49</sup> two non-reactive force fields (Optimized Potentials for Liq-

uid Simulations, OPLS<sup>51</sup> and Consistent Valence Force Field, CVFF<sup>52</sup>) and seven different ReaxFF parameterizations were tested for PPTA and PAP5. The results indicated that the ReaxFF force field developed by Liu<sup>53</sup> was best for studying structure-property relationships of PPTA and PAP5. Since the structure of PAP6, PAP7, and PAP8 are similar to PPTA and PAP5, we used ReaxFF with the Liu force field for the simulations here.

All the MD simulations were carried out using the open-source MD simulation package LAMMPS (Large-scale Atomic/Molecular Massively Parallel Simulator).<sup>54</sup> OVITO (Open Visualization Tool)<sup>55</sup> was used for model visualization. The MD time step was 0.25 fs for all simulations. Temperature and pressure were controlled using a Nosé-Hoover thermostat<sup>56</sup> and barostat<sup>57</sup> with damping parameters of 25 fs and 250 fs, respectively. Energy minimization was performed after the unit cells were replicated. Then, each polymer crystal was equilibrated by running simulations in the NPT (constant number of atoms, pressure, and temperature) ensemble for 125 ps (until the lattice parameters reached steady state) at 300 K and 1 atm. The unit cell lattice parameters of the equilibrated polymers are shown in Table S2. The magnitude of the unit cell dimensions,  $a$ ,  $b$ , and  $c$ , each changed by about 2% on average after NPT equilibration. The largest single change was a 4.5% decrease in the  $a$  dimension of PAP5. The unit cells remain nearly monoclinic but take on some triclinic character. The lattice angles  $\alpha$  and  $\beta$  each change by about 4% on average remain between 80° and 90°. The largest change in the unit cell parameters is in  $\gamma$ , which decreases by 1% for PPTA and 14% on average for the four aromatic-aliphatic polyamides. In summary, the chain packing in the backbone and H-bonded directions are only modestly changed, while the  $\pi$ - $\pi$  stacking planes are sheared slightly for an average decrease in unit cell volume of 1% for PPTA and 6% for the aromatic-aliphatic polyamides. Next, the system was stretched in the chain direction (x-direction) with a strain rate of  $1 \times 10^9 \text{ s}^{-1}$  until the total strain reached 25% (true strain). The details of the method were reported in our previous paper.<sup>49</sup> The low-strain elastic modulus was calculated by applying a linear fit to the stress-strain data from 0-2% strain, and the high-strain modulus was calculated from the last 5% strain before

failure. The ultimate stress was the stress at the failure strain. These simulations were repeated three times independently with different random velocity seeds before the NPT simulation.

Lastly, a separate set of simulations was run to model the stress-strain response of individual polyamide chains. All the chains, except the one in the center of the crystal, were removed from the last trajectory of each  $4 \times 4 \times 4$  model after equilibration in the NPT ensemble. Then, strain was applied to the single chain in the x-direction using the same approach as described above for the crystals until 25% true strain was reached.

## Results and Discussion

The stress response of each aromatic-aliphatic polyamide crystal to strain in the chain-direction is shown in Figure 2a. The moduli of the crystals are shown in Figure 2b. All crystals exhibited strain hardening, transitioning from a low-strain linear regime to a high-strain linear regime. In Figure 2b, the low-strain and high-strain moduli are plotted as functions of the number of non-aromatic carbons in the polymer repeating unit. At high-strain, the modulus is essentially independent of the number of non-aromatic carbon atoms. This result is consistent with the fact that, at high strain, the modulus is mediated by deformation of covalent backbone bonds, and the bond stiffnesses are similar in all five polymers.

In contrast, the low-strain modulus decreases with increasing number of non-aromatic carbon atoms (Figure 2b). In our previous study of PPTA and PAP5,<sup>49</sup> we found that low strain behavior could be correlated with chain waviness (a simple average metric related to the departure from fully extended chain conformations) because wavy chains can accommodate strain without deformation of covalent bonds. Waviness can be quantified from the distribution of the atoms in the polymer in the plane transverse to the chain direction, i.e., the yz plane. Figure 3a is a representative plot of the positions of the non-aromatic backbone



atoms in PAP7 with respect to the centroid of each chain, from zero strain to failure. At low strain (darker blue), the atoms are far from the centroid, indicating a wavy structure. Then, as strain increases (lighter blue), the chain is extended, and the atoms are found closer to the centroid. Similar behavior was exhibited by the other polymers (see Figure S1)

Waviness was calculated as the radius of a circle that encompasses 90% of the atomic coordinates closest to the center of the chain such that a larger radius corresponds to atoms further scattered from the centroid and wavier chain. The results for all polymers are shown in Figure 3b, where waviness at 0% strain,  $R_0$ , increases with number of non-aromatic carbons. To confirm the use of a radius to approximate distribution size was reasonable even for non-circular atom position distributions, we also calculated the area of an oval fit to the positions of the 90% innermost non-aromatic carbon atoms and nitrogen atoms. Like the radius, the area of the best-fit oval increased with number of non-aromatic carbons (see Figure S4). The increasing trend of waviness is due to the methylene groups acting as spacers between the hydrogen-bonded amide groups, which increases the conformational freedom of the polymer chains.<sup>11,58</sup> The strong negative correlation between the low-strain modulus and waviness is shown in Figure 3b.

In Figure 2, except for PPTA, all of the polymers exhibit a change in slope between low and high strain in the stress-strain curve. Also, for some polymers, there is a second inflection or shoulder, after the slope change, in the stress-strain curve. To explore the origin of this behavior, stress-strain simulations were performed for single chains taken from the end of the NPT equilibration simulation of each crystal before stretching. Two representative comparisons between crystals and single chains, for PAP6 and PAP7, are shown in Figure 4. Both single chains and crystals exhibit lower stiffness at low strain than at high strain, with the increase in stiffness occurring around 5% strain, indicating that this behavior is due to intra-chain processes. For PAP6 (Figure 4a) and PAP8 (Figure S2e), the second inflection or shoulder after the initial slope change in the stress-strain curve is only observed for the crystals, not the single chains. This indicates that the second transition in the stress-strain

response of the even polymers is due to inter-chain effects.

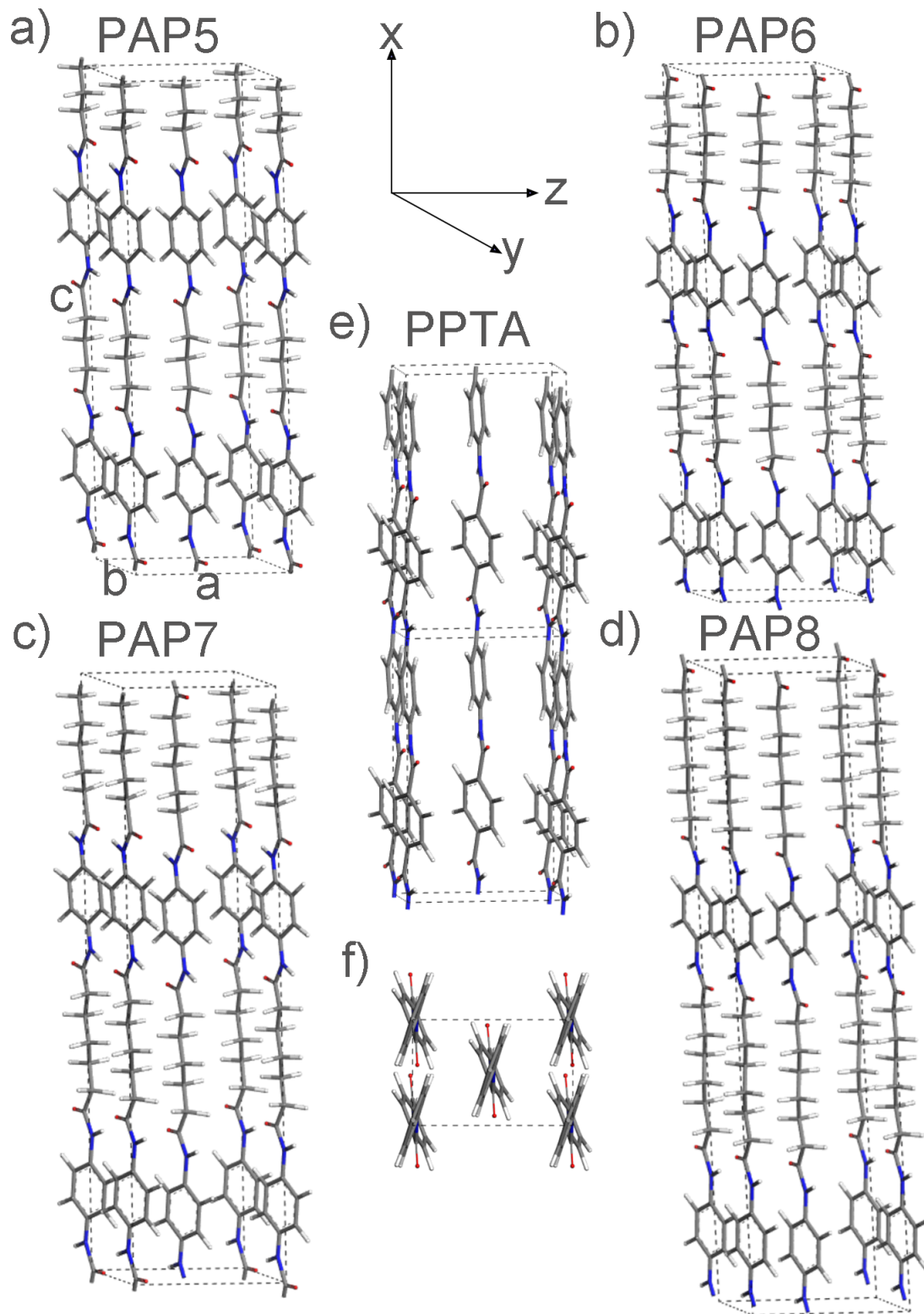


Figure 1: Initial unit cells of (a) PAP5, (b) PAP6, (c) PAP7, (d) PAP8, and (e-f) PPTA. The orthogonal directions ( $x$ ,  $y$ , and  $z$ ) and lattice constants ( $a$ ,  $b$ , and  $c$ ) are defined with respect to the perspective view of the PPTA. Atom colors correspond to: oxygen, red; nitrogen, blue; carbon, gray; and hydrogen, white.

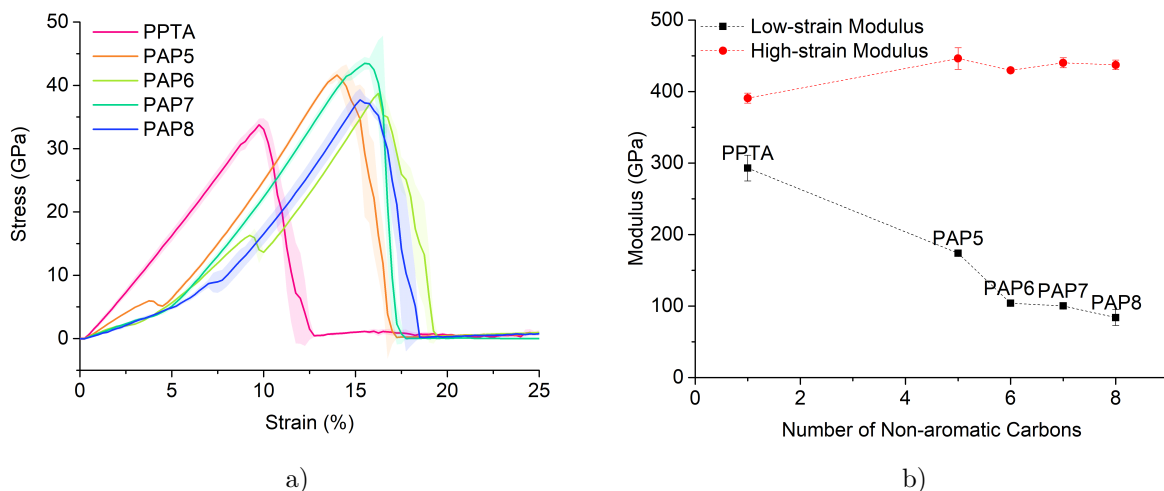


Figure 2: (a) Stress-strain curves for  $4 \times 4 \times 4$  polyamide crystals strained from 0 to 25% strain. The shaded areas reflect standard deviations calculated from three independent simulations. (b) Low-strain and high-strain modulus as functions of the number of non-aromatic carbons in the polymer repeating unit. Low-strain modulus is calculated from the slope of stress-strain curve from 0 to 2% strain. High-strain modulus is calculated from the last 5% strain before failure. Dotted lines are guides to the eye.

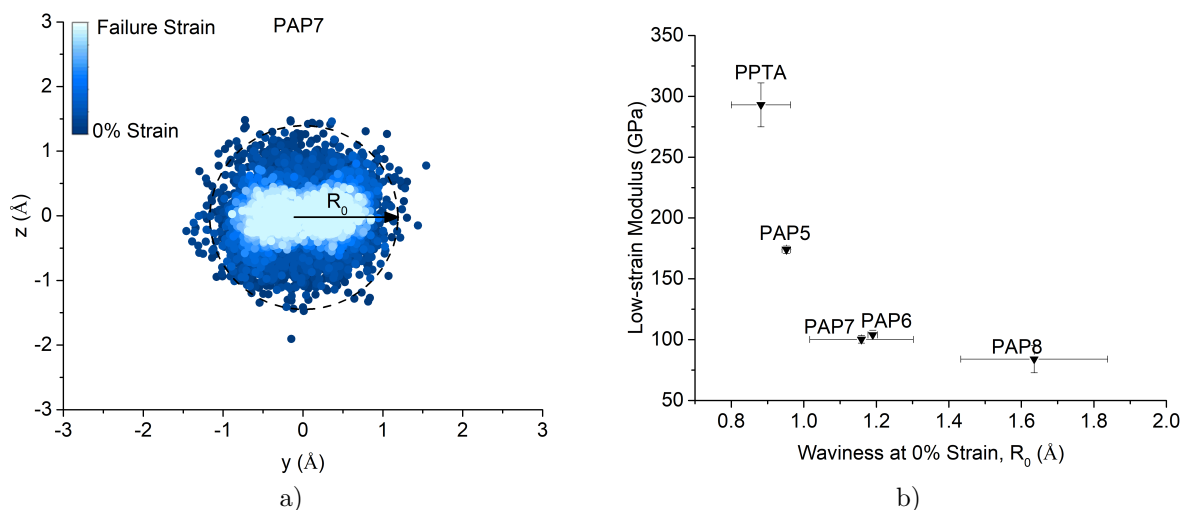


Figure 3: (a) Positions of atoms in the chains projected on the yz plane for PAP7 as a function of strain, where the origin corresponds to the centroid of each chain. Similar plots for the other polymers are shown in Figure S1. Waviness is quantified as the radius  $R_0$  of a circle encompassing the coordinates of 90% of the inner-most non-aromatic carbon atoms and nitrogen atoms. (b) Low-strain modulus as a function of the waviness at 0% strain. The error bars reflect the standard deviations calculated from three independent simulations.

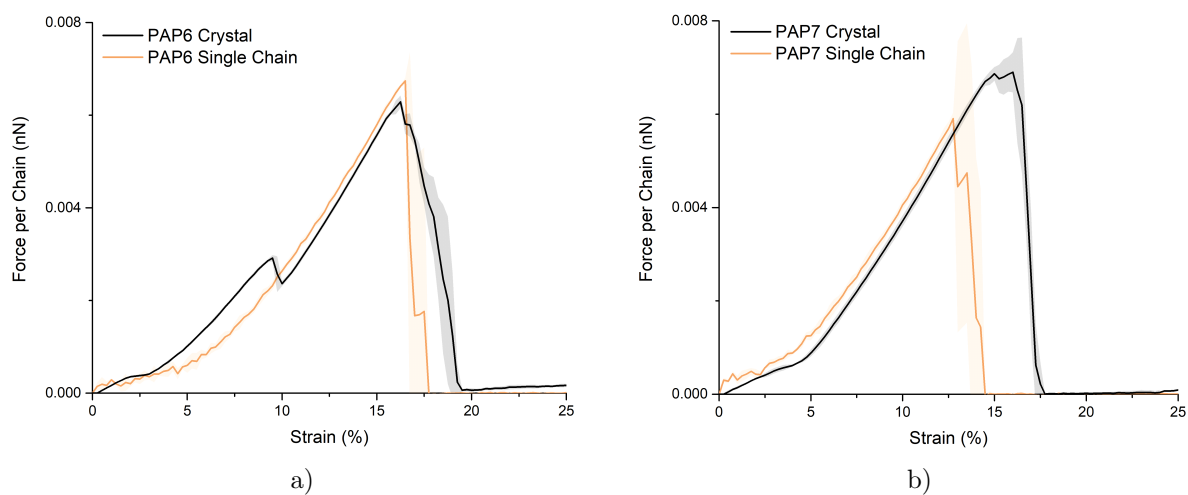


Figure 4: Stress-strain response of single chain (orange) and crystal (black) forms of (a) PAP6 and (b) PAP7. The single chain is taken from the end of the NPT equilibration simulation of each crystal before stretching. The force per chain is calculated as the total stress multiplied by the cross-sectional area of the simulation box (orthogonal to the strain direction) and then divided by 32 chains for the crystal and 1 for the single chain. Similar trends for PAP5 and PAP8 are shown in Figure S2. The shaded areas reflect standard deviations calculated from three independent simulations.

To understand how inter- and intra-chain interactions affect the stress-strain response of the crystals, the movement of the atoms and aromatic rings was characterized in terms of rotation of dihedral angles and inter-chain slip. First, dihedral rotation was quantified as the dihedral angles (HNCO, NCCC, and OCCC) in the backbones of the chains. The change of the dihedral angles during stretching relative to the equilibrated state at zero strain is plotted as a function of strain in Figure 5. For PAP5-PAP8, the NCCC dihedral angles increase and the OCCC angles decrease gradually in the low-strain regime as the energy barriers for bond rotations are overcome.<sup>24</sup> The gradual increase in stiffness at low-strain exhibited by all polymers, except PPTA, correlates well with changes in the dihedral angles, indicating that small strains are accommodated by straightening wavy chains, i.e., backbone bond rotation. Then, the dihedral angles abruptly increase to near  $180^\circ$  or decrease to near  $0^\circ$ , corresponding to full extension of the chains, and remain constant until failure. The strain at which these rotational modes are exhausted corresponds closely with the transition out of the low-strain regime for all four aromatic-aliphatic polyamides. In contrast, PPTA adopts the lowest energy fully extended (all-trans) conformation at zero strain, and thus does not undergo conformational rearrangements under tensile deformation.

The predominant inter-chain mechanism observed in the simulations is slip between the chains within each hydrogen-bonded sheet. Inter-chain slip was quantified by the change of average distance (relative to the zero strain distance) in the x-direction between the centers of mass of each pair of adjacent aromatic rings stacked in the z-direction. For PPTA, PAP5, and PAP7, the slip remains at zero until failure. However, for PAP6 and PAP8 (animations in Movie S1), the chains undergo a discrete slipping event (the magnitude of which is  $\sim 0.5$  Å) at the strain corresponding to the second inflection point in the stress data. After this slip event, the relative positions of the chains remain stable until failure.

The key morphological difference between the even and odd polyamides is the geometry of the H-bonding. The even polymers exhibit a parallelogram H-bonding structure that is less stable than the trapezoid structure of polymers with an odd number of carbon atoms;<sup>59-61</sup> see

Figure S5 for representative snapshots of these structures. This so-called odd-even effect<sup>59,62</sup> has been observed in the elastic properties of polymers including  $\alpha,\omega$ -alkanedicarboxylic acids<sup>63</sup> and polyesters.<sup>64,65</sup> The greater stability of the odd polymers manifests in the strain dependence of the crystal unit cell lattice parameter in the H-bonding direction,  $b$  (see Figure 1a for lattice parameter assignments). As shown in Figure 6a, tension in the chain direction caused compression of the lattice in the H-bonding direction for all polymers, corresponding to a gradual decrease of  $b$  with strain. This decrease continued for the odd polymers until failure. However, for the even polymers, the lattice constant  $b$  abruptly increased at the strain at which inter-chain slip was observed, and then decreased again until failure. The abrupt change of lattice constant  $b$  with strain for PAP6 and PAP8 is consistent with the H-bonding trends. A comparison between the average H-bond length and  $\pi$ - $\pi$  slip in Figure S6 shows that the H-bond length change occurs immediately before the  $\pi$ - $\pi$  slip for PAP6 and PAP8. This indicates that the  $\pi$ - $\pi$  slip is driven by an abrupt change in the configuration of the H-bonded sheets.

Odd-even effects have also been observed in ultimate properties.<sup>64,66</sup> As shown in Figure 6b, aromatic-aliphatic polyamides with an even number of carbon atoms have lower ultimate stresses. In all cases the reactive simulations predict that failure occurs by breaking the N-C(O) bond in the amide. Density functional theory (DFT) calculations were used to probe the bond dissociation energies (BDEs) of the N-C(O) in single repeat units of PPTA and a representative fragment of an aromatic-aliphatic polyamide (Figure S7). The DFT results showed that the aliphatic segment does not affect bond strength, suggesting the observed odd-even trend in ultimate stress is an inter-chain effect.

Figure 4 and Figure S6 clearly implicate intermolecular interactions for the enhanced strength of the odd polymers. The odd polymer crystals exhibit higher strains and stresses per chain at failure than their single-chain counterparts; on the contrary, the failure properties of the crystals and single chains of the even polymers are indistinguishable. The less stable H-bond structure of the even polymers is one contributing factor. In Figure 6a, prior

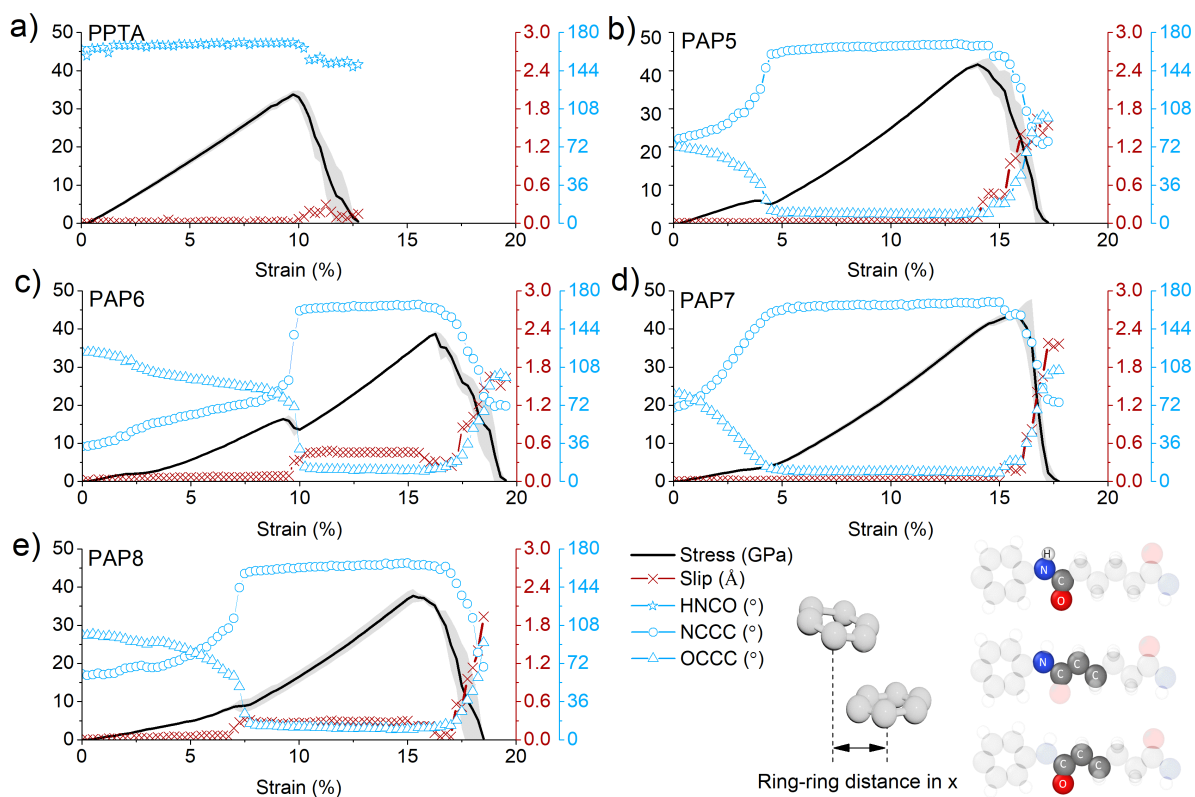


Figure 5: Stress, inter-chain slip, and dihedral angles as functions of strain of (a) PPTA, (b) PAP5, (c) PAP6, (d) PAP7, and (e) PAP8. Two of the carbons in the NCCC and OCCC dihedrals are aliphatic and one is the amide carbonyl. Data is shown only until failure for each crystal. Illustrations of the ring-ring distance and the dihedral angles are shown in the lower right corner of the figure. The HNC0 dihedral angle distributions are similar for the different polymers ( $158 \pm 7^\circ$ ) at low strains. This angle increases slightly with increasing strain before failure, but the change is very small compared to that exhibited by the other dihedral angles (see Figure S3).

to failure, the lattice constants  $b$  of even polymers are larger than those of the odd polymers, implying that the H-bonds are correspondingly weaker and thus H-bonding contributes less to resisting failure in the even polymers.

It has also been shown that ring-ring interactions ( $\pi$ -stacking) affect the ultimate properties of polyamides, and the strength of these interactions is related to the coplanarity of the rings.<sup>49,67</sup> The coplanarity of the rings is quantified here by the angle between each pair of aromatic rings in adjacent chains (see inset to Figure 6b) averaged over the last 2% strain before failure. Coplanarity is plotted as a function of the number of non-aromatic carbons in



the polymer repeating unit in Figure 6b, where small ring-ring angles correspond to better registry between the aromatic rings (high coplanarity). The ultimate stress and coplanarity of the polymers exhibit consistent trends where polymers with poorer registry (weaker  $\pi$ - $\pi$  interactions) have lower strength. The less stable inter-chain interactions of the even polymers is also seen in Figure S2 where the force per chain and failure strain are significantly higher in crystals vs. single chains for odd polymers (PAP5 and PAP7), but there is no statistical difference for even polymers (PAP6 and PAP8).

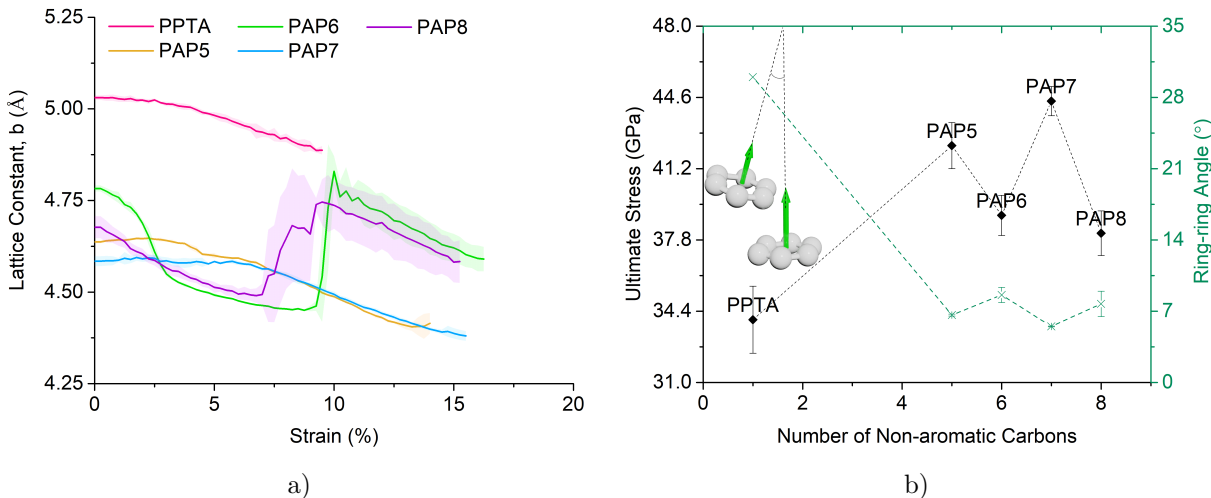


Figure 6: (a) Lattice constant in the H-bonding direction,  $b$ , for the polymer crystals as a function of strain in the x-direction (chain direction). Data is shown only until failure for each crystal. The shaded areas and errors bars reflect standard deviations from three independent simulations. (b) Ultimate stress and ring-ring angle (averaged over the last 2% before the stress drop for each polymer) as functions of the number of non-aromatic carbons in the polymer repeating unit. The inset schematic defines ring-ring angle.

Finally, it is important to note that the stresses in the simulations are higher than those achievable in experiments.<sup>40,68–71</sup> This is because our model systems have aligned infinite chains (single crystal) without defects (e.g., no chain ends or impurities) or nucleation sites for fracture, which maximizes material strength. In addition, higher order structures that are present in real materials, such as fibrils, amorphous material, as well as chain and/or crystal misorientation, are expected to negatively affect the mechanical properties. Nonetheless, the trends reported here reflect limiting behavior and can be used to understand the effect of the

alkyl chain length. Further, the high strain rates of the simulations are necessitated by the inherently short timescale of the simulation method,<sup>1,72-74</sup> and have been reported to result in higher predicted strength and modulus. This strain rate-dependence has been attributed to the (in)commensurability between the rate of deformation and the frequency of molecular processes.<sup>5</sup> Although only a limited strain rate range could be tested in the simulations due to the short timescale inherent to reactive force fields, we performed stress-strain simulations for the crystals at two additional strain rates,  $1 \times 10^8 \text{ s}^{-1}$  and  $1 \times 10^{10} \text{ s}^{-1}$ . As shown in Figure S8, the transitions from low- to high-strain regimes shifted to higher stresses with increasing strain rate, which is qualitatively consistent with the effect of strain rate on the yield point of semicrystalline<sup>75</sup> and amorphous polymers.<sup>76,77</sup> However, the trends exhibited by calculated mechanical properties, shown in Figure S9, were similar at the three strain rates. Specifically, at all strain rates tested, the low-strain modulus decreased with increasing number of non-aromatic carbons, the high-strain moduli were insensitive to the number of non-aromatic carbons and were higher than the low-strain moduli, and the ultimate stress exhibited odd-even effect.

## Conclusions

Molecular dynamics simulations were performed to study the stress-strain response of PPTA and four related aromatic-aliphatic polyamides with different numbers of non-aromatic carbons in the polymer repeating unit. Two distinct linear stress-strain regimes were observed. It was found that the subtle differences between these polymers lead to distinct elastic and ultimate properties. The low-strain modulus (calculated from 0-2% strain) decreased with increasing aliphatic chain length while the high-strain modulus (calculated from the last 5% strain before failure) was independent of the aliphatic chain length. The trend of low-strain modulus was explained in terms of the departure from the extended chain conformations—waviness—of the polymers at zero strain. Longer aliphatic chains increased the

conformational freedom of the chains and thus the waviness of the polymers, which finally decreased the low-strain modulus. The transition from low to high strain behavior was correlated with changing of dihedral angles as the chains were extended, so this behavior was due to intra-chain effects. It was also observed that polymers with an even number of non-aromatic carbon atoms exhibited a discrete inter-chain slip mechanism at the transition between the wavy and extended conformation, which was explained by the instability of the H-bonding structure in these polymers. A similar odd-even effect was observed at failure, where even polymers had lower ultimate stress. Coplanarity of the aromatic rings correlated well with the trend of ultimate stress, i.e., less coplanar rings (larger ring-ring angle) corresponded to lower ultimate stress.

Generally, the results reported here show that aromatic-aliphatic polyamides can be designed with mechanical properties comparable to or better than PPTA, yet even subtle differences in chemical composition can have strong implications for the mechanical response. Further, the correlations between structure and mechanical properties identified herein, as well as the simulation-based approach, may be extended to other similar polymers to enable tuning of mechanical properties through chemical modification.

## Supporting Information

Movies including the strain simulations of all polymers shown from the y-direction (H-bond direction, Movies S1) and x-direction (chain-direction, Movies S2). Tables including the initial unit cell lattice parameters of the polymers (Table S1) and post-NPT unit cell lattice parameters of the polymers (Table S2). Figures including positions of the non-aromatic, backbone atoms in the chains projected on the yz plane (Figure S1); stress-strain response of single chain and crystal forms (Figure S2); stress and HNCO dihedral angle as functions of strain (Figure S3); waviness of the polymers calculated as the radius of best fit circle and the cross-sectional area of the chains calculated from of the best fit oval of the atom distribution

(Figure S4); representative snapshots of trapezoid and parallelogram structures in the backbones of odd and even polymers and corresponding H-bonds (Figure S5); average H-bond length (N-O distance) and inter-chain slip during stretching (Figure S6); truncated polymer models used to compute the bond dissociation energy (BDE) (Figure S7); stress-strain curves of the polyamides at three different strain rates (Figure S8); mechanical properties as functions of the number of non-aromatic carbons in the polymer repeating units at three different strain rates (Figure S9).

## Acknowledgement

We acknowledge ExxonMobil Research and Engineering Company for financial support of this work. The stimulating discussions with ExxonMobil colleagues (Ozcan Altintas, Arben Jusufi, Agostino Pietrangelo, Thomas Sun, Loan T. Vo, Pamela J. Wright) are highly appreciated. The simulations were in part run using the Extreme Science and Engineering Discovery Environment (XSEDE), which is supported by National Science Foundation Grant ACI-1548562.

## References

- (1) Shim, V.; Lim, C.; Foo, K. Dynamic mechanical properties of fabric armour. *International Journal of Impact Engineering* **2001**, *25*, 1–15.
- (2) Knijnenberg, A.; Bos, J.; Dingemans, T. J. The synthesis and characterisation of reactive poly (p-phenylene terephthalamide) s: a route towards compression stable aramid fibres. *Polymer* **2010**, *51*, 1887–1897.
- (3) Yang, H. *Kevlar aramid fiber*; Wiley, 1993.
- (4) Mark, H.; Atlas, S.; Ogata, N. Aromatic polyamide. *Journal of Polymer Science* **1962**, *61*, S49–S53.

- (5) Sockalingam, S.; Chowdhury, S. C.; Gillespie Jr, J. W.; Keefe, M. Recent advances in modeling and experiments of Kevlar ballistic fibrils, fibers, yarns and flexible woven textile fabrics—a review. *Textile Research Journal* **2017**, *87*, 984–1010.
- (6) Kim, J.; McDonough, W. G.; Blair, W.; Holmes, G. A. The modified-single fiber test: A methodology for monitoring ballistic performance. *Journal of applied polymer science* **2008**, *108*, 876–886.
- (7) Krishnan, K.; Sockalingam, S.; Bansal, S.; Rajan, S. Numerical simulation of ceramic composite armor subjected to ballistic impact. *Composites Part B: Engineering* **2010**, *41*, 583–593.
- (8) Rao, Y.; Waddon, A.; Farris, R. Structure–property relation in poly (p-phenylene terephthalamide)(PPTA) fibers. *Polymer* **2001**, *42*, 5937–5946.
- (9) Hogg, P. J. Composites in armor. *Science* **2006**, *314*, 1100–1101.
- (10) Brauckmann, J. O.; Zolfaghari, P.; Verhoef, R.; Klop, E. A.; de Wijs, G. A.; Kentgens, A. P. Structural studies of polyaramid fibers: Solid-state NMR and first-principles modeling. *Macromolecules* **2016**, *49*, 5548–5560.
- (11) Deshmukh, Y. S.; Wilsens, C. H.; Verhoef, R.; Hansen, M. R.; Dudenko, D.; Graf, R.; Klop, E. A.; Rastogi, S. Conformational and structural changes with increasing methylene segment length in aromatic–aliphatic polyamides. *Macromolecules* **2016**, *49*, 950–962.
- (12) Chen, X. *Advanced fibrous composite materials for ballistic protection*; Woodhead Publishing, 2016.
- (13) Dobb, M.; Johnson, D.; Majeed, A.; Saville, B. Microvoids in aramid-type fibrous polymers. *Polymer* **1979**, *20*, 1284–1288.

- (14) Debeaupre, E.; Watanabe, M.; Sanui, K.; Ogata, N. In situ polycondensation for synthesis of composites of elastomeric matrixes and wholly aromatic polyamides. *Chemistry of materials* **1992**, *4*, 1123–1128.
- (15) Ferreiro, J. J.; de La Campa, J. G.; Lozano, A. E.; de Abajo, J. Polyisophthalamides with heteroaromatic pendent rings: synthesis, physical properties, and water uptake. *Journal of Polymer Science Part A: Polymer Chemistry* **2005**, *43*, 5300–5311.
- (16) Ferrero, E.; Espeso, J.; De la Campa, J.; De Abajo, J.; Lozano, A. Synthesis and characterization of aromatic polyamides containing alkylphthalimido pendent groups. *Journal of Polymer Science Part A: Polymer Chemistry* **2002**, *40*, 3711–3724.
- (17) Zhou, S.; Zhang, M.; Wang, R.; Ping, J.; Zhang, X.; Zhao, N.; Xu, J.; Shen, Z.; Fan, X. Synthesis and characterization of new aramids based on o-(m-triphenyl)-terephthaloyl chloride and m-(m-triphenyl)-isophthaloyl chloride. *Polymer* **2017**, *109*, 49–57.
- (18) García, J. M.; García, F. C.; Serna, F.; José, L. High-performance aromatic polyamides. *Progress in polymer science* **2010**, *35*, 623–686.
- (19) Huang, Y.-C.; Wang, K.-L.; Chang, C.-H.; Liao, Y.-A.; Liaw, D.-J.; Lee, K.-R.; Lai, J.-Y. Solvent Response and Protonation Effects of Novel Aramides Containing Pyridine and Unsymmetrical Carbazole Moieties. *Macromolecules* **2013**, *46*, 7443–7450.
- (20) Morgan, P.; Kwolek, S. Polyimides from phenylenediamines and aliphatic diacids. *Macromolecules* **1975**, *8*, 104–111.
- (21) Rutledge, G.; Suter, U.; Papaspyrides, C. Analysis of structure of polymorphism in poly (p-phenyleneterephthalamide) through correlation of simulation and experiment. *Macromolecules* **1991**, *24*, 1934–1943.
- (22) Crouch, I.; Arnold, L.; Pierlot, A.; Billon, H. *The science of armour materials*; Elsevier, 2017; pp 269–330.

- (23) Brown, J.; Ennis, B. Thermal analysis of Nomex® and Kevlar® fibers. *Textile Research Journal* **1977**, *47*, 62–66.
- (24) Tonelli, A. E.; Edwards, J. F. Are poly (p-phenylene terephthalamide)(Kevlar®) and other liquid crystalline polymers conformationally rigid? *Polymer* **2020**, *193*, 122342.
- (25) Khademinejad, S.; Mehdipour-Ataei, S.; Ziaee, F.; Abbasi, F. Poly (ether ether sulfone amide) s as a new category of processable heat-resistant polymers. *Designed Monomers and Polymers* **2016**, *19*, 553–559.
- (26) Liou, G.-S.; Fang, Y.-K.; Yen, H.-J. Synthesis and properties of noncoplanar rigid-rod aromatic polyamides containing phenyl or naphthyl substituents. *Journal of Polymer Research* **2007**, *14*, 147–155.
- (27) Amininasab, S. M.; Rashidi, A.; Taghavi, M.; Shami, Z. Preparation and characterization of novel thermostable polyamides bearing different photoactive pendent architectures with antibacterial properties. *Chinese Journal of Polymer Science* **2016**, *34*, 766–776.
- (28) Hajibeygi, M.; Shabaniyan, M.; Khodaei-Tehrani, M. New heat resistant nanocomposites reinforced silicate nanolayers containing triazine rings based on polyamide: synthesis, characterization, and flame retardancy study. *Polymer Composites* **2016**, *37*, 188–198.
- (29) Zou, F.; Wen, H.; Yan, T.; Cai, M. Synthesis and properties of novel soluble aromatic polyamides containing 4-aryl-2, 6-diphenylpyridine moieties and pendant fluorinated phenoxy groups. *Journal of Polymer Research* **2016**, *23*, 1–10.
- (30) Zhang, G.; Yan, G.-M.; Ren, H.-H.; Li, Y.; Wang, X.-J.; Yang, J. Effects of a trans- or cis-cyclohexane unit on the thermal and rheological properties of semi-aromatic polyamides. *Polymer Chemistry* **2016**, *7*, 44–53.

- (31) Damaceanu, M.-D.; Rusu, R.-D.; Nicolescu, A.; Bruma, M.; Rusanov, A. L. Organosoluble asymmetric aromatic polyamides bearing pendent phenoxy groups. *Polymer international* **2011**, *60*, 1248–1258.
- (32) Long, J.-W.; Chen, L.; Liu, B.-W.; Shi, X.-H.; Lin, X.-B.; Li, Y.-M.; Wang, Y.-Z. Tuning the Pendent Groups of Semiaromatic Polyamides toward High Performance. *Macromolecules* **2020**, *53*, 3504–3513.
- (33) Peng, S.; Peng, L.; Yi, C.; Zhang, W.; Wang, X. A novel synthetic strategy for preparing semi-aromatic components modified polyamide 6 polymer. *Journal of Polymer Science Part A: Polymer Chemistry* **2018**, *56*, 959–967.
- (34) Bakkali-Hassani, C.; Planes, M.; Roos, K.; Wirotius, A.-L.; Ibarboure, E.; Carlotti, S. Synthesis of polyamide 6 with aramid units by combination of anionic ring-opening and condensation reactions. *European Polymer Journal* **2018**, *102*, 231–237.
- (35) Rwei, S.-P.; Ranganathan, P.; Chiang, W.-Y.; Lee, Y.-H. Synthesis and characterization of copolyamides derived from novel aliphatic bio-based diamine. *Journal of Applied Polymer Science* **2018**, *135*, 46878.
- (36) Rwei, S.-P.; Ranganathan, P.; Chiang, W.-Y.; Lee, Y.-H. Synthesis of low melting temperature aliphatic-aromatic copolyamides derived from novel bio-based semi aromatic monomer. *Polymers* **2018**, *10*, 793.
- (37) Bisoi, S.; Mandal, A. K.; Padmanabhan, V.; Banerjee, S. Aromatic polyamides containing trityl substituted triphenylamine: Gas transport properties and molecular dynamics simulations. *Journal of Membrane Science* **2017**, *522*, 77–90.
- (38) Li, M. Study on melting and polymorphic behavior of poly (decamethylene terephthalamide). *Journal of Polymer Science Part B: Polymer Physics* **2019**, *57*, 465–472.



- (39) Prevorsek, D. C.; Kwon, Y. D.; Chin, H. B. Analysis of the temperature rise in the projectile and extended chain polyethylene fiber composite armor during ballistic impact and penetration. *Polymer Engineering & Science* **1994**, *34*, 141–152.
- (40) Cline, J.; Wu, V.; Moy, P. *Assessment of the Tensile properties for single fibers*; 2018.
- (41) Baughman, R.; Gleiter, H.; Sendfeld, N. Deformation and microstructure of extended-chain polydiacetylene crystals. *Journal of Polymer Science: Polymer Physics Edition* **1975**, *13*, 1871–1879.
- (42) Wu, G.; Tashiro, K.; Kobayashi, M. Vibrational spectroscopic study on molecular deformation of polydiacetylene single crystals: stress and temperature dependences of Young’s modulus. *Macromolecules* **1989**, *22*, 188–196.
- (43) Nakamoto, S.; Tashiro, K.; Matsumoto, A. Vibrational spectroscopic study on the molecular deformation mechanism of a poly (trans-1, 4-diethyl muconate) single crystal subjected to tensile stress. *Macromolecules* **2003**, *36*, 109–117.
- (44) Tashiro, K.; Kobayashi, M.; Tadokoro, H. Elastic moduli and molecular structures of several crystalline polymers, including aromatic polyamides. *Macromolecules* **1977**, *10*, 413–420.
- (45) Moe, N. E.; Ediger, M. Molecular dynamics computer simulation of polyisoprene local dynamics in dilute toluene solution. *Macromolecules* **1995**, *28*, 2329–2338.
- (46) Zhang, B.; Liu, R.; Zhang, J.; Liu, B.; He, J. MesoDyn simulation study of phase behavior for dye–polyether derivatives in aqueous solutions. *Computational and Theoretical Chemistry* **2016**, *1091*, 8–17.
- (47) Zhelavskiy, O. S.; Kyrychenko, A. Atomistic molecular dynamics simulations of the LCST conformational transition in poly (N-vinylcaprolactam) in water. *Journal of Molecular Graphics and Modelling* **2019**, *90*, 51–58.

- (48) Chantawansri, T. L.; Yeh, I.-C.; Hsieh, A. J. Investigating the glass transition temperature at the atom-level in select model polyamides: A molecular dynamics study. *Polymer* **2015**, *81*, 50–61.
- (49) Yang, Q.; Li, W.; Stober, S. T.; Burns, A. B.; Gopinadhan, M.; Martini, A. Molecular Dynamics Simulation of the Stress–Strain Behavior of Polyamide Crystals. *Macromolecules* **2021**, *54*, 8289–8302.
- (50) BIOVIA, BIOVIA Material Studio. 2020; <http://www.3ds.com/products-services/biovia/products/molecular-modeling-simulation/biovia-materials-studio>, Last accessed 16 February 2021.
- (51) Dodda, L. S.; Cabeza de Vaca, I.; Tirado-Rives, J.; Jorgensen, W. L. LigParGen web server: an automatic OPLS-AA parameter generator for organic ligands. *Nucleic acids research* **2017**, *45*, W331–W336.
- (52) Dauber-Osguthorpe, P.; Roberts, V. A.; Osguthorpe, D. J.; Wolff, J.; Genest, M.; Hagler, A. T. Structure and energetics of ligand binding to proteins: Escherichia coli dihydrofolate reductase-trimethoprim, a drug-receptor system. *Proteins: Structure, Function, and Bioinformatics* **1988**, *4*, 31–47.
- (53) Liu, L.; Liu, Y.; Zybin, S. V.; Sun, H.; Goddard III, W. A. ReaxFF-ig: Correction of the ReaxFF reactive force field for London dispersion, with applications to the equations of state for energetic materials. *The Journal of Physical Chemistry A* **2011**, *115*, 11016–11022.
- (54) Plimpton, S. Fast parallel algorithms for short-range molecular dynamics. *Journal of computational physics* **1995**, *117*, 1–19.
- (55) Stukowski, A. Visualization and analysis of atomistic simulation data with OVITO—the Open Visualization Tool. *Modelling and Simulation in Materials Science and Engineering* **2009**, *18*, 015012.

- (56) Hoover, W. G. Canonical dynamics: Equilibrium phase-space distributions. *Physical review A* **1985**, *31*, 1695.
- (57) Hoover, W. G. Constant-pressure equations of motion. *Physical Review A* **1986**, *34*, 2499.
- (58) Hansen, M. R.; Graf, R.; Spiess, H. W. Solid-state NMR in macromolecular systems: insights on how molecular entities move. *Accounts of chemical research* **2013**, *46*, 1996–2007.
- (59) Thalladi, V. R.; Nüsse, M.; Boese, R. The melting point alternation in  $\alpha$ ,  $\omega$ -alkanedicarboxylic acids. *Journal of the American Chemical Society* **2000**, *122*, 9227–9236.
- (60) White, N. A.; Ellis, H. A. Room temperature structures and odd–even behaviour of a homologous series of anhydrous lithium n-alkanoates. *Journal of Molecular Structure* **2008**, *888*, 386–393.
- (61) Bond, A. D. On the crystal structures and melting point alternation of the n-alkyl carboxylic acids. *New journal of chemistry* **2004**, *28*, 104–114.
- (62) Baeyer, A. Ueber regelmässigkeiten im schmelzpunkt homologer verbindungen. *Berichte der deutschen chemischen Gesellschaft* **1877**, *10*, 1286–1288.
- (63) Mishra, M. K.; Varughese, S.; Ramamurty, U.; Desiraju, G. R. Odd–even effect in the elastic moduli of  $\alpha$ ,  $\omega$ -alkanedicarboxylic acids. *Journal of the American Chemical Society* **2013**, *135*, 8121–8124.
- (64) Shen, Y.; Yao, B.; Yu, G.; Fu, Y.; Liu, F.; Li, Z. Facile preparation of bio-based polyesters from furandicarboxylic acid and long chain diols via asymmetric monomer strategy. *Green Chemistry* **2017**, *19*, 4930–4938.

- (65) Flores, I.; Pérez-Camargo, R. A.; Gabirondo, E.; Caputo, M. R.; Liu, G.; Wang, D.; Sardon, H.; J, M. A. Unexpected Structural Properties in the Saturation Region of the Odd–Even Effects in Aliphatic Polyethers: Influence of Crystallization Conditions. *Macromolecules* **2022**,
- (66) Prisacariu, C.; Scortanu, E. Influence of the type of chain extender and urethane group content on the mechanical properties of polyurethane elastomers with flexible hard segments. *High Performance Polymers* **2011**, *23*, 308–313.
- (67) Burattini, S.; Greenland, B. W.; Hayes, W.; Mackay, M. E.; Rowan, S. J.; Colquhoun, H. M. A supramolecular polymer based on tweezer-type  $\pi$ -  $\pi$  stacking interactions: molecular design for healability and enhanced toughness. *Chemistry of Materials* **2011**, *23*, 6–8.
- (68) Cheng, M.; Chen, W.; Weerasooriya, T. Experimental investigation of the transverse mechanical properties of a single Kevlar® KM2 fiber. *International Journal of Solids and Structures* **2004**, *41*, 6215–6232.
- (69) Lim, J.; Zheng, J. Q.; Masters, K.; Chen, W. W. Effects of gage length, loading rates, and damage on the strength of PPTA fibers. *International Journal of Impact Engineering* **2011**, *38*, 219–227.
- (70) Dobb, M.; Johnson, D.; Saville, B. Compressional behaviour of Kevlar fibres. *Polymer* **1981**, *22*, 960–965.
- (71) Rao, Y.; Waddon, A.; Farris, R. The evolution of structure and properties in poly (p-phenylene terephthalamide) fibers. *Polymer* **2001**, *42*, 5925–5935.
- (72) Zhu, D.; Mobasher, B.; Rajan, S. D. Dynamic tensile testing of Kevlar 49 fabrics. *Journal of materials in civil engineering* **2011**, *23*, 230–239.

- (73) Thomas, J. A.; Shanaman, M. T.; Lomicka, C. L.; Boyle, M. P.; Calderon-Colon, X.; LaBarre, E. D.; Tiffany, J. E.; Trexler, M. M. Multiscale modeling of high-strength fibers and fabrics. *Micro-and Nanotechnology Sensors, Systems, and Applications IV*. 2012; p 83731S.
- (74) Lomicka, C.; Thomas, J.; LaBarre, E.; Trexler, M.; Merkle, A. *Dynamic Behavior of Materials, Volume 1*; Springer, 2014; pp 187–193.
- (75) Lim, S.-H.; Yu, Z.-Z.; Mai, Y.-W. Effects of loading rate and temperature on tensile yielding and deformation mechanisms of nylon 6-based nanocomposites. *Composites Science and Technology* **2010**, *70*, 1994–2002.
- (76) Brulé, B.; Halary, J. L.; Monnerie, L. Molecular analysis of the plastic deformation of amorphous semi-aromatic polyamides. *Polymer* **2001**, *42*, 9073–9083.
- (77) Ho, J.; Govaert, L.; Utz, M. Plastic deformation of glassy polymers: correlation between shear activation volume and entanglement density. *Macromolecules* **2003**, *36*, 7398–7404.

# TOC Graphic

